Structural Engineering and Mechanics, *Vol. 69, No. 5 (2019) 499-509*
DOI: https://doi.org/10.12989/sem.2019.69.5.499

Development of optimum modeling approach in prediction of wheelflats effects on railway forces

Javad Sadeghi*[1a], Amin Khajehdezfuly[2a], Morteza Esmaeili[1a] and Davood Poorveis[2a]

[1]*School of Railway Engineering, Iran University of Science and Technology, Tehran, Iran*
[2]*Department of Civil Engineering, Faculty of Engineering, Shahid Chamran University of Ahvaz, Ahvaz, Iran*

(Received December 1, 2018, Revised December 22, 2018, Accepted January 15, 2019)

Abstract. While the wheel flat is an asymmetrical phenomenon in the railway, majority of researches have used two-dimensional models in the investigation of the effect of wheel flat on the wheel rail forces. This is due to the considerably low computational costs of two dimensional (2D) models although their reliability is questionable. This leaves us with the question of "what is the optimum modeling technique?". It is addressed in this research. For this purpose, two and three dimensional numerical models of railway vehicle/track interaction were developed. The three dimensional (3D) model was validated by comparisons of its results with those obtained from a comprehensive field tests carried out in this research and then, the results obtained from the 2D and 3D models were compared. The results obtained indicate that there are considerable differences between wheel/rail forces obtained from the 2D and 3D models in the conditions of medium to large wheel-flats. On the other hand, it was shown that the results of the 2D models are reliable for particular ranges of vehicle speed, railway track stiffness and wheel-fats lengths and depths. The results were used to draw a diagram, which presents the optimum modeling technique, compromising between the costs and accuracy of the obtained results.

Keywords: wheel-flat; three and two dimensional; numerical model; nonlinear Hertz contact

1. Introduction

The contact force between wheels and rails is one of the main factors in the railway track design (Askarinejad and Dhanasekar 2016, Yan *et al.* 2018, Sadeghi *et al.* 2016a, Sadeghi *et al.* 2016b, Jansseune and De Corte 2017, Xia *et al.* 2018, Kahya and Araz 2017). The wheel-flat can cause substantial intensification of wheel/rail forces (Gandhi *et al.* 2015, Kouroussis *et al.* 2015, Guo *et al.* 2017 and Zhu *et al.* 2009). Severe train's brakes cause development of wheel flats in the wheel (Handoko and Dhanasekar 2006). Wheel flats induce severe dynamic forces, causing nonlinear damage accumulation in the rail (Kreiser *et al.* 2007). Therefore, detection of wheel flats and investigation of their effects on the track responses are important in the railway research (Jia and Dhanasekar 2007). Mostly, wheel flat is asymmetric about the center of the railway track (Zhu *et al.* 2009 and Steenbergen 2007). For instance, while a wheel flat has been found on the right wheel, the left one is intact (Zhu *et al.* 2009 and Steenbergen 2007). The influence of the wheel-flat on the wheel/rail force has been investigated by two and three dimensional numerical models in the available literature. In the two dimensional (2D) model, a symmetry condition is considered in the track, and consequently, half of the track is simulated. This causes considerably less computational cost in the 2D models compared with the three dimensional (3D) ones (Zou *et al.* 2016, Sadeghi *et al.* 2016b). Therefore, despite the fact that the wheel flat is known as an asymmetrical phenomenon, various two 2D numerical models have been developed for the investigation of the effect of wheel flat on the wheel rail forces. Newton and Clark were the first to investigate the effect of wheel-flat on the wheel/rail force using a 2D model (Newton and Clark 1979). In their model, the railway track was simulated as a beam rested on an elastic foundation, the vehicle was modeled as a moving mass and the wheel/rail contact was considered as a nonlinear Hertz spring. They evaluated the accuracy of their theoretical results by conducting field measurements. Due to the limitations of solving the nonlinear problem in the frequency domain, the vehicle/track interaction problem with nonlinear Hertz spring has been usually investigated in the time domain (Yang *et al.* 1999). Further use of 2D models for the investigation of the effect of a single wheel-flat on the wheel rail forces has been made by several researchers (Thompson *et al.* 2003, Wu and Thompson 2004, Nielsen and Igeland 1995, Zhai *et al.* 2001, Sun and Dhanasekar 2002, Uzzal *et al.* 2008 and Uzzal 2012). In most of these studies, the wheel/rail contact was considered as a nonlinear Hertz spring and the wheel-flat was assumed as a half-cosine wave shape irregularity on the top of the rail.

Although the amounts of flatness of the left and right wheels are mostly different (asymmetric wheel flats), the left and right sides of the railway track and the vehicle are assumed the same in the 2D models (Zhu *et al.* 2009 and Steenbergen 2007). This assumption might cause some errors in the 2D models results (Uzzal *et al.* 2009). Due to

*Corresponding author, Professor
E-mail: javad_sadeghi@iust.ac.ir
[a]Ph.D.

ISSN: 1225-4568 (Print), 1598-6217 (Online)

the limitation of the 2D models in the consideration of asymmetric wheel flats, some 3D models have been developed in the literature (Uzzal *et al.* 2009). For instance, Uzzal *et al.* developed a 3D model of vehicle/ballasted track interaction problem to investigate the effects of different wheel-flats of the right and left wheels of a wheel set on the vehicle response (Uzzal *et al.* 2013). In their model, the vehicle was simulated as a wagon with seventeen degrees of freedom (DOF), the wheel/rail contact was considered as a nonlinear Hertz spring, and the track (composed of left rail, right rail and sleepers) was modeled as a two layered system. This model was further used to investigate the effects of the multiple wheel-flats of one wheel and two wheels on the vehicle response (Uzzal *et al.* 2014).

In spite of considerably less computational costs of 2D models, it has been proved that the 2D models provide less accurate results compared to the 3D models (Sadeghi *et al.* 2016b). However, it is not clear to which extend (or conditions) the 2D models are unreliable. In other word, an important question of "what is the optimum modeling technique to have the minimum computational cost while having sufficient accuracy?" has been left unanswered (Hamdoon *et al.* 2011, Nasr *et al.* 2018 and Shallan *et al.* 2018). This indicates that there is a need to investigate the effectiveness of 2D models in accurate prediction of the effects of various single of asymmetric wheel-flats on the wheel-rail contact force. In response to this need, 2D and 3D models of vehicle/track interaction problem were developed in this study. These models consider wheel/rail contact as a nonlinear Hertz spring and their solutions are based on Newmark integration method in conjunction with full Newton-Raphson incremental-iterative scheme (Sadeghi *et al.* 2016c). This solution method has the best performance from the aspect of its computational cost among others available in the literature (Sadeghi *et al.* 2016c). The validation of results obtained by the models was made by comparisons of the results obtained from the models with those of experiments carried out in this study. Through a parametric study of the vehicle speed, track stiffness and wheel-flat length and depth, the level of accuracy, reliability, and cost effectiveness of the 2D and 3D modeling techniques in the estimation of the effects of asymmetric single wheel-flats on wheel/rail contact forces were investigated, leading to propose an optimum modeling technique.

2. Development of numerical models

In order to investigate the effects of asymmetric single wheel-flats on wheel/rail contact forces, 2D and 3D numerical models of railway vehicle/track interaction were developed. The longitudinal and side views of the 3D model are presented in Figs. 1 and 2, respectively. As illustrated in Figs. 1 and 2, the track in the 3D model is composed of right and left rails and a supporting system. The rails were modeled using the Timoshenko beam elements (Przemieniecki 1985, Edem 2006) and the supporting system was simulated using the spring/dashpot elements (Sadeghi *et al.* 2016b). Wheel-flats cause high frequency excitation. According to the literature, shear deformation

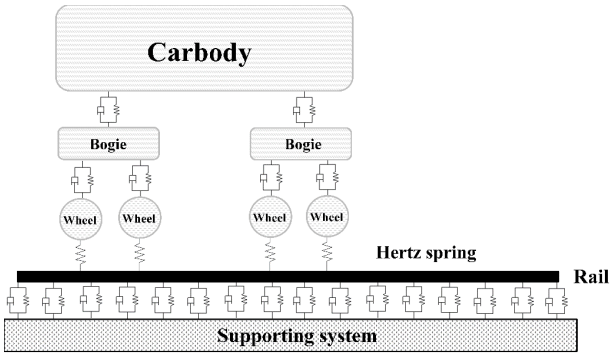

Fig. 1 Longitudinal view of the 3D and 2D models

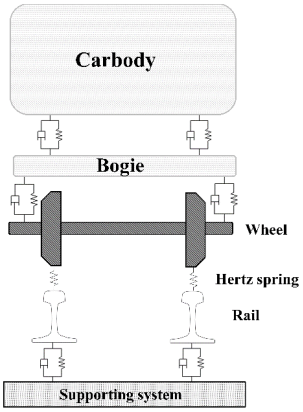

Fig. 2 Cross section view of the 3D model

should be considered in the ranges of high frequency excitation. Therefore, the rail is modeled as Timoshenko beam element in order to consider the effect of shear deformation on the rail response. The rails were connected discontinuously to the subgrade (as a supporting system). The vehicle in the 3D model was modeled as a wagon with seventeen degree of freedom (DOF) (Kumaran *et al.* 2002).

A view of the 2D model is presented in Fig. 1. In the 2D model, the rail and supporting system were modeled using the Timoshenko beam elements and the spring/dashpot elements, respectively. The vehicle of the 2D model was simulated as a wagon with ten DOF (Sadeghi and Fesharaki 2013). The equation of motion of the vehicle and the track for both models (2D and 3D model) was written in Eq. (1), where K, C and M are the stiffness, damping and mass matrices of the whole system, respectively. The acceleration, velocity and displacement vectors of system are defined as $\ddot{X}$, $\dot{X}$ and X respectively and F is the force vector.

$$\boldsymbol{KX + C\dot{X} + M\ddot{X} = F} \tag{1}$$

The wheel/rail contact was considered as a nonlinear Hertz spring as formulated in Eq. (2) (Newton and Clark 1979), where $F^{H}_{int_m}$ is the wheel/rail contact force, C_H is the Hertz spring constant, z_{w_m} is the vertical displacement of the wheel, z_{r_m} is the rail displacement at the wheel-rail contact point in the vertical direction, and z_{d_m} is the rail irregularity.

In the 3D model, the sub-index "m" is "1" for the right

wheel and "2" for the left wheel. It is considered "1" for the 2D model (Uzzal *et al.* 2013).

$$F_{int_m}^{H} = \begin{cases} C_H\left(z_{w_m} - z_{r_m} - z_{d_m}\right)^{\frac{3}{2}} = C_H(dZ_m)^{\frac{3}{2}} & z_{w_m} - z_{r_m} - z_{d_m} > 0 \\ 0 & z_{w_m} - z_{r_m} - z_{d_m} \le 0 \end{cases} \quad (2)$$

In the 3D model, the wheel vertical displacement (z_{w_m}) was calculated using Eq. (3) in terms of the wheelset DOF, the vertical displacement (Z_{ws}) and the rotation ($\emptyset_{ws}$) about the longitudinal axis. In Eq. (3), b is the track gauge. The wheel vertical displacement (z_{w_1}) is denoted by Z_{ws} in the 2D model (Sadeghi *et al.* 2016b and Uzzal *et al.* 2013).

$$z_{w_m} = Z_{ws} + \text{sign} \times \frac{b}{2} \times sin(\emptyset_{ws}) \quad \text{sign} = \begin{cases} +1 & m = 1 \\ -1 & m = 2 \end{cases} \quad (3)$$

The governing differential equation of motions of the vehicle and the track (Eq. (1)) in both models (2D and 3D) was modified in order to incorporate the effect of the nonlinear Hertzian spring force. For this purpose, the internal virtual work of the Hertzian spring in the contact point at the analysis time $t + \Delta t$ ($(\delta w_{int}^{H})_{t+\Delta t}$) was written as in Eq. (4) (Borst *et al.* 2012).

$$(\delta w_{int}^{H})_{m}^{t+\Delta t} = C_H\left(z_{w_m} - z_{r_m} - z_{d_m}\right)^{\frac{3}{2}} . \left(\delta Z_{w_m} - \delta Z_{r_m}\right) \quad (4)$$

where C_H, z_{w_m}, z_{r_m} and z_{d_m} are as described earlier and δZ_{w_m} and δZ_{r_m} are the virtual displacements of the wheel and the rail in the contact point, respectively. Z_r was discretized by using the linear interpolation functions, φ_k (k=1-4), as follows (Przemieniecki 1985)

$$z_{r_m} = \sum_{k=1}^{4} z_{r_m}^{k} \times \varphi_i \quad (5)$$

where $Z_{r_m}^{1}$, $Z_{r_m}^{3}$ are the vertical DOF of the rail element nodes i and j, respectively and $Z_{r_m}^{2}$, $Z_{r_m}^{4}$ are the rotational DOF of the rail element nodes i and j, respectively. i and j are the first and end points of the beam element, respectively. The rotational degree of freedom is independent from translation degree of freedom (Edem 2006). The linear form of $\left(\delta w_{int}^{H}\right)_{m}^{t+\Delta t}$ for the left and right sides of the 3D model can be written as under (Borst *et al.* 2012)

$$\begin{aligned} &(\delta w_{int}^{H}(\boldsymbol{g}, \delta \boldsymbol{g}))_{m}^{t+\Delta t} \\ &= (\delta w_{int}^{H}(\boldsymbol{g}, \delta \boldsymbol{g}))_{m}^{t} \\ &+ D[(\delta w_{int}^{H}(\boldsymbol{g}, \delta \boldsymbol{g}))]_{m}^{t} \Delta \boldsymbol{g} \end{aligned} \quad (6)$$

where g, δg and Δg are the displacement, virtual displacement and incremental displacement vectors, respectively. g is the vector of the wheel and the rail element DOF in the contact point in the 3D model as defined under

$$\boldsymbol{g} = \{Z_{ws} \quad \emptyset_{ws} \quad Z_{r_1}^{1} \quad Z_{r_1}^{2} \quad Z_{r_1}^{3} \quad Z_{r_1}^{4} \quad Z_{r_2}^{1} \quad Z_{r_2}^{2} \quad Z_{r_2}^{3} \quad Z_{r_2}^{4}\}^{T} \quad (7)$$

In the 2D model, Eq. (6) was used when sub-index m takes "1". In addition, in 2D model the vector g is modified as follows

$$\boldsymbol{g} = \{Z_{ws} \quad Z_{r_1}^{1} \quad Z_{r_1}^{2} \quad Z_{r_1}^{3} \quad Z_{r_1}^{4}\}^{T} \quad (8)$$

where, $D\left[\left(\delta w_{int}^{H}(g, \delta g)\right)\right]_{m}^{t} \Delta g$, is the directional derivative of the internal virtual work of the Hertzian spring in the δg direction (Borst *et al.* 2012). Eq. (6) was rewritten in the following form (Eq. (9)) in order to derive the Hertzian internal force vector and the Hertzian tangent stiffness matrix (Borst *et al.* 2012).

$$(\delta w_{int}^{H}(\boldsymbol{g}, \delta \boldsymbol{g}))_{m}^{t+\Delta t} = \delta \boldsymbol{g}^{T} \boldsymbol{F}_{int}^{H} + \delta \boldsymbol{g}^{T} \boldsymbol{K}_{T}^{H} \Delta \boldsymbol{g} \quad (9)$$

where F^H and K_T^H are the Hertzian internal force vector and the Hertzian tangent stiffness matrix, respectively. In the 3D model, they were defined as Eq. (10). In Eq. (10), $K_T^H(n, o)$ is the component of the nth row and the oth column of the tangent stiffness matrix K_T^H, and $F^H(n)$ is the nth component of the Hertzian internal force vector F^H. Using Eqs. (10), the effect of nonlinear Hertz spring between the wheel and the rail was taken into the governing differential equation of motions of the whole system in the 3D model (Eq. (10)). In the 2D model, sub-index m takes 1 and the DOF of components of Hertzian internal force vector and the Hertzian tangent stiffness matrix were modified according to Eq. (8). In Eq. (10), the values of k and p are changed from 1 to 4.

$$\begin{aligned} K_T^H(z_{ws}, z_{ws}) &= \sum_{m=1}^{2} \left(\frac{3}{2} C_H (dz_m)^{1/2}\right)_m \\ K_T^H(\emptyset_{ws}, \emptyset_{ws}) &= \sum_{m=1}^{2} \left(\left[-\text{sign} \times \frac{b}{2} \times \sin(\emptyset_{ws}) \times F_H\right] \right. \\ &\quad + \left[\frac{3}{2} C_H (dz_m)^{1/2} \left(\text{sign} \times \frac{b}{2} \right.\right. \\ &\quad \left.\left. \times \sin(\emptyset_{ws})\right)^2\right] \Big)_m \\ K_T^H(z_{ws}, \emptyset_{ws}) &= \sum_{m=1}^{2} \left(\text{sign} \times \frac{b}{2} \times \cos(\emptyset_{ws}) \right. \\ &\quad \left. \times \frac{3}{2} C_H (dz_m)^{1/2}\right)_m \\ K_T^H(z_{ws}, z_r^k) &= \sum_{m=1}^{2} \left(-\varphi_k \times \frac{3}{2} C_H (dz_m)^{1/2}\right)_m \\ K_T^H(\emptyset_{ws}, z_r^k) &= \sum_{m=1}^{2} \left(-\text{sign} \times \frac{b}{2} \times \cos(\emptyset_{ws}) \times \varphi_k \right. \\ &\quad \left. \times \frac{3}{2} C_H (dz_m)^{1/2}\right)_m \\ K_T^H(z_r^k, z_r^p) &= \sum_{m=1}^{2} \left(\varphi_k \times \varphi_l \times \frac{3}{2} C_H (dz_m)^{1/2}\right)_m \\ F^H(z_{ws}) &= \sum_{m=1}^{2} \left(F_{int}^{H}\right)_m \end{aligned} \quad (10)$$

$$F^{H}(\emptyset_{ws}) = \sum_{m=1}^{2}\left(\text{sign} \times \frac{b}{2} \times \cos(\emptyset_{ws}) \times F_{int}^{H}\right)_{m}$$

$$F^{H}(z_{r}^{k}) = \sum_{m=1}^{2}\left(-\varphi_{k} \times F_{int}^{H}\right)_{m}$$

The governing differential equations of the vehicle and the track motions in both models, with the consideration of the wheel/rail contact as a nonlinear Hertz spring, were derived and solved in the time domain. A new solution algorithm developed by these authors (Sadeghi *et al.* 2016c) was used to solve the equations of the motions of both models in the time domain and in a coupled form. The solution algorithm is a combination of the Newmark-Beta integration method and the full Newton-Raphson iterative scheme (Sadeghi *et al.* 2016c and Borst *et al.* 2012).

3. Validation of 3D numerical model

To evaluate the accuracy of the 3D model results, a comparison was made between the results obtained from the model and those of field measurements. For this purpose, comprehensive field test was carried out in this research. Because of the dominant effect of the rail displacement on the wheel/rail contact force (as in Eq. (2)), the rail displacement was considered as an appropriate criterion for the comparison. The tests were performed in the Iranian largest metro network (in the capital city). A view of the field test location (near Shahid Zeino-Din station) is presented in Fig. 3. The slab track in the field was Rehda-2000 with UIC54 rail lied on a concrete bed with stiffness and damping of 100 MN/m and 0.2 MN.s/m, respectively. The fastening space was 0.6 m.

In order to consider the worst scenario, the test was performed on a part of the track which had a non-symmetric rail irregularity. That is, a half-sine irregularity was observed on the right rail head while the left rail has no irregularity. As shown in Fig 4, the irregularity of the right rail is located in the mid-span of the rail between two fastening system. The right rail irregularity amplitude and wavelength are 0.15 m and 2.5 mm, respectively. A view of the left rail condition is presented in Fig. 5. The metro train includes seven wagons (each has four axles). The axle load was 14 ton. Properties of the vehicle were obtained from Tehran metro car manufacture (CNR 2002). A view of the train at the test location is presented in Fig. 6 (a). The tests were made when the train passed with the speed of 25 km/hr. A view of the train wheel on the rail is shown in Fig. 6 (b).

Four Linear Variable Displacement Transducers (LVDTs) were used to record the right and left rails deflections and the absolute slab displacements. A schematic view of the LVDTs arrangement is presented in Fig. 7. The first LVDT (LVDT1) was used to record the relative displacement of the right rail to the slab (near the irregularity point). The second LVDT (LVDT2) was used to record the absolute deflection of the slab at the right side of the track. From the data obtained from LVDT1 and LVDT2, the absolute vertical displacement of the right rail

Fig. 3 Field test location

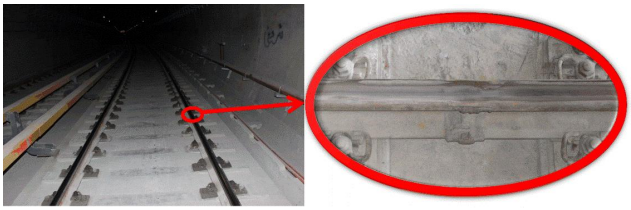

Fig. 4 Right rail with irregularity

Fig. 5 Left rail without irregularity

(a) View of the train used in the test

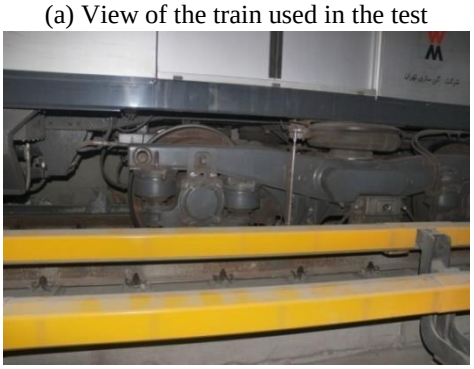

(b) Train wheel running on the rail

Fig. 6 Views of train running on the rail

was derived. Similarly, the absolute deflection of the left rail was derived from the data obtained from LVDT3 (recording the relative deflection of the rail to the slab) and LVDT4 (recording the absolute defection of the slab). A view of LVDTs installation on the field test is presented in

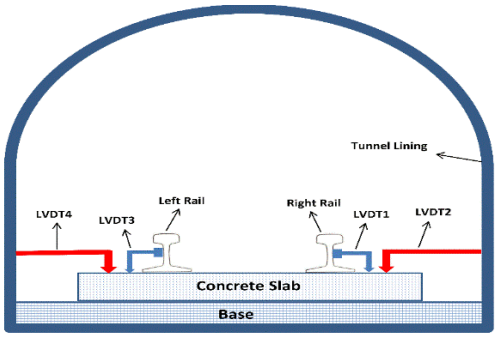

Fig. 7 Left rail without irregularity

(a) On the left rail

(b) On the right rail

Fig. 8 Installation of LVDTs on the rails

Fig. 8. A data logger namely TMR-211 was used to record the data measured by LVDTs. A view of TMR-211 data recorder is presented in Fig. 9. The data obtained by the TMR-211 was transferred to a Laptop computer and processed using the TMR software (Fig. 9). The 3D model was run, taking into consideration the properties of the track and the vehicle (as the model input parameters). The vertical displacement of the right and left rails obtained from the model for the vehicle speed of 25 km/hr are compared with those of the field test in Figs. 10 and 11. The results were obtained when the fourth wagon was passed over the LVDTs positions.

Based on the results presented in Fig. 10, the maximum displacements of the left rail under the first and the second bogies are 0.78 mm and 0.83 mm, respectively. That is, the left rail displacements for the first and the second bogies are

(a) Measurement on the site

(b) Data logger TMR-211

Fig. 9 Field measurement using TMR-211 data logger

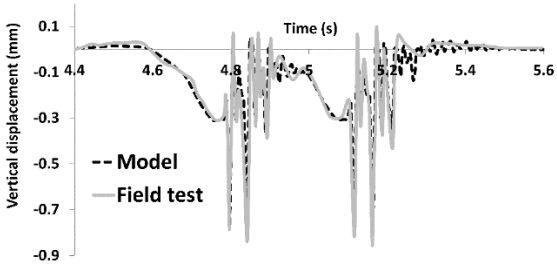

Fig. 10 Left rail vertical displacement

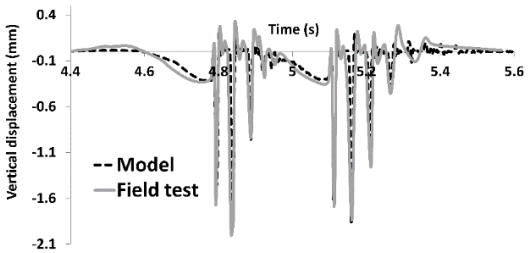

Fig. 11 Right rail vertical displacement

nearly the same (with 2% deference). The differences between the results obtained from the model and the measurement are in the range of (3-4%), having its maximum under the second bogie. The time history of the right rail displacement is presented in Fig. 11. As indicated in this figure, the maximum displacement of the right rail (which had irregularity) is about 1.99 mm. Comparison of the results presented in Figs. 10 and 11 shows that the

Table 1 Wheel-flats properties

Wheel flat condition	Length (mm)	Depth (mm)
Small	20	0.05
Medium	150	1.5
Large	100	0.9
Very large	150	2.15

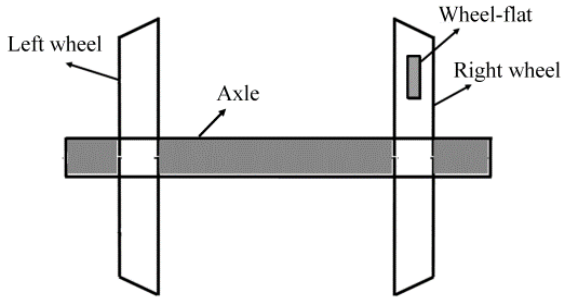

Fig. 12 Schematic view of asymmetric wheel-flat condition

maximum vertical displacement of the left rail is 50% lower than that of the right rail, indicating the considerable effects of the asymmetric rail irregularity on the results. As illustrated in these figures, the results obtained from the 3D model are in good agreement with those of the field test (having at the most 8% difference). In other word, the 3D model is reliable to predict the effect of asymmetric wheel-flat on the wheel rail force.

4. Reliability of 2D model in various wheel flatness conditions

In order to investigate the reliability of the 2D modeling technique in the estimation of the effects of asymmetric single wheel-flats on the wheel/rail contact forces, the results obtained from the 2D model (developed in Section 2) were compared with those of the 3D model validated in Section 3. The comparisons were made when there is asymmetric wheel flats condition. A schematic view of asymmetric wheel flats conditions is shown in Fig. 12. In the asymmetric wheel-flat condition (Fig. 12), the wheel-flat is considered on the right wheel of the 3D model. Moreover, a wheel-flat was considered only on the first wheel of the vehicle in the 2D model. Four types of single wheel-flats (very large, large, medium and small) were considered in this study (Table 1) (obtained from Uzzal *et al.* 2013).

The wheel-flat was considered as a half cosine rail irregularity in the middle of the rail as indicated in Eq. (11) where $Z_d(x)$, d and l are the rail irregularity at the location x, the wheel-flat depth, and the wheel-flat length, respectively (Newton and Clark 1979).

$$Z_d(x) = \frac{d}{2}\left(1 - \cos\left(\frac{2\pi x}{l}\right)\right) \quad (11)$$

In the 3D model, the track was considered as two rails with UIC60 profile (Molatefi and Izadbakhsh 2013) laid on

Table 2 Supporting system properties

Supporting system type	Stiffness ($\frac{MN}{m}$)	Damping ($\frac{N.s}{m}$)
Low stiffness	25	2×10^4
Medium stiffness	150	6×10^4
High stiffness	250	1×10^5

Table 3 Vehicle properties

Parameter	magnitude
Car body mass	58400 kg
Bogie mass	3600 kg
Wheelset mass	1900 kg
Mass moment of inertia of the car body about x axis	95576 $kg.m^2$
Mass moment of inertia of the car body about y axis	726462 $kg.m^2$
Mass moment of inertia of the bogie about x axis	1600 $kg.m^2$
Mass moment of inertia of the bogie about y axis	1801 $kg.m^2$
Mass moment of inertia of the wheel-set about x axis	420.1 $kg.m^2$
Primary suspension stiffness	788000 kN/m
Primary suspension damping	3500 $N.s/m$
Secondary suspension stiffness	5320 kN/m
Secondary suspension damping	70000 $N.s/m$
Longitudinal distance between bogies	10.36 m
Longitudinal distance between wheel-sets in bogie	2.5 m
Lateral distance between secondary suspensions	1.6 m
Lateral distance between primary suspensions	1.6 m
Hertz spring constant	87000000 $kN/m^{3/2}$

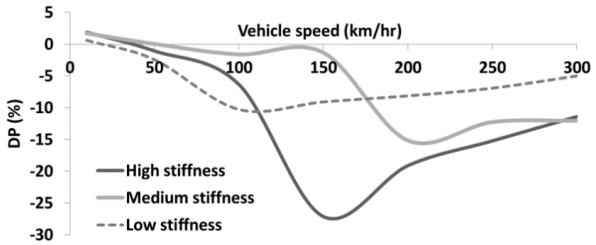

Fig. 13 DP in asymmetric small wheel-flat condition

the supporting system with properties presented in Table 2 (obtained from Egana *et al.* 2006). The sleeper spacing was 600 mm. As it is presented in Table 2, three different scenarios (supporting system with low stiffness, medium stiffness and high stiffness) were considered for the supporting system properties. The ranges of supporting system stiffness considered in the parametric study are in the ranges of equivalent stiffness of ballasted and slab tracks. Therefore, the results obtained from the parametric study are applicable in different types of railway superstructure such as ballasted or slab track. The number of time steps of each analysis was 6000. Six Timoshenko

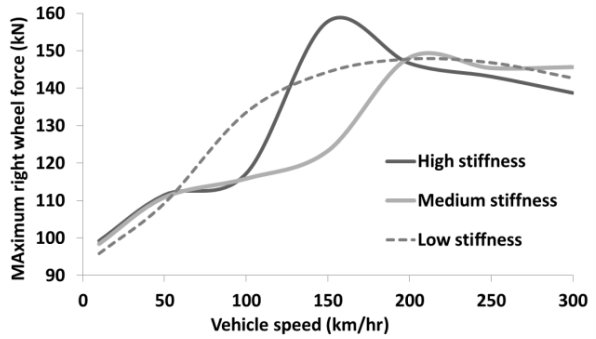

(a) Right wheel

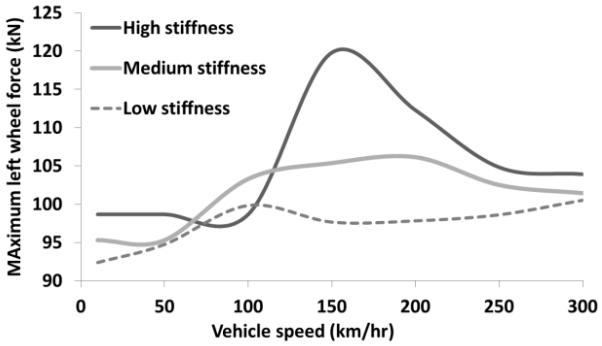

(b) Left wheel

Fig. 14 Maximum wheel/rail force of first wheel in asymmetric small wheel-flat condition obtained from 3D model

beam elements were used to simulate the rail between two fastening systems.

In the 2D model, half of the track and the vehicle were simulated. The wagon with the properties presented in Table 3 (obtained from Uzzal *et al.* 2013) was run with the speeds in the ranges of (10-300 km/hr). The DOF of the 2D and 3D models were 402 and 821, respectively. The difference between the maximum wheel/rail forces obtained from the 2D and 3D model was considered as the main criterion in the comparisons. This was due to the fact that wheel flat has a significant effect on the maximum magnitude of the wheel/rail force known as the main factor of inducing stress and deflection in the railway track components. In order to evaluate the reliability of the 2D model in unsymmetrical wheel flatness conditions, an index called DP (wheel/rail force Differences in Percentage) is defined to compare the maximum of wheel/rail force obtained from the 2D model with that of the 3D model (See Eq. (12)). In Eq. (12), F_{max}^{2D} and $F_{max}^{3d,rw}$ are the maximum wheel/rail force obtained from the 2D model and the right wheel/rail force obtained from the 3D model, respectively.

$$DP = \frac{F_{max}^{2D} - F_{max}^{3D,rw}}{F_{max}^{3D,rw}} \times 100 \quad (12)$$

The DP in asymmetric small wheel-flat condition is presented in Fig. 13. Moreover, the maximum wheel/rail force obtained from the 3D model for the left and right wheels are presented in Fig. 14. As illustrated in Fig. 13, at the vehicle speed lower than 30 km/hr, DP is positive and consequently the maximum wheel/rail force obtained from the 2D model is more than that of the 3D model. However, the DP is negative and subsequently the maximum wheel/rail force obtained from the 2D model is lower than that of the 3D model for the vehicle speed of more than 30 km/hr.

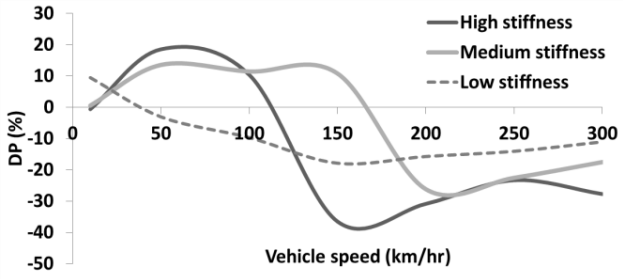

Fig. 15 DP in asymmetric medium wheel-flat condition

According to Fig. 13 (the case of small wheel-flat condition and low track stiffness), when the vehicle speed is changed, the variation of DP is negligible compared with those of the medium and high track stiffness. Fig. 14 indicates that as the small wheel-flat condition is considered on the right wheel, the maximum wheel/rail force for the right wheel is more than that of the left. Based on Fig. 13, the DP for the vehicle speed of 150 km/hr and a high stiffness of the track support reaches almost 30 percent. As illustrated in Fig. 14, the maximum wheel/rail force in high stiffness tracks has a maximum at the vehicle speed of 150 km/hr. It means that as the track stiffness is increased, the variation of vehicle speed has more influence on the DP variation. In the other word, when the track stiffness is high (see Table 2), the capability of the 2D model to predict the effect of asymmetric wheel-flat on the wheel/rail force is decreased as the vehicle speed is increased. Moreover, in case of the medium and high track stiffness, when the vehicle speed is increased, the DP is increased and therefore, the 2D model is not sufficiently reliable for prediction of the effects of asymmetric small wheel-flat on the wheel/rail force.

The influence of the medium wheel-flat on the DP is presented in Fig. 15. As indicated in this figure, the difference between the results obtained from the 2D and 3D models were increased when the wheel-flat size was changed from small to medium. Moreover, the effect of the medium wheel-flat on the maximum wheel/rail force obtained from the 3D model is illustrated in Fig. 15. As presented in Fig. 15, when the track stiffness is increased, the DP is increased and therefore, the 2D model perdition is less reliable. The variation of graphs presented in Fig. 16(a) is roughly the same as that of Fig. 14 (medium wheel-flat condition in the 2D model). As an interesting point, based on Fig. 16, when the vehicle speed is less than 200 km/hr, the maximum wheel/rail force on the left wheel is affected by the wheel-flat considered on the right wheel, but when the vehicle speed is more than 200 km/hr, the left wheel maximum wheel/rail force is not influenced by the wheel-flat. In other words, when the vehicle speed is more than 200 km/hr, the wheel-flat on the right wheel does not have any influence on the maximum wheel/rail force of the left

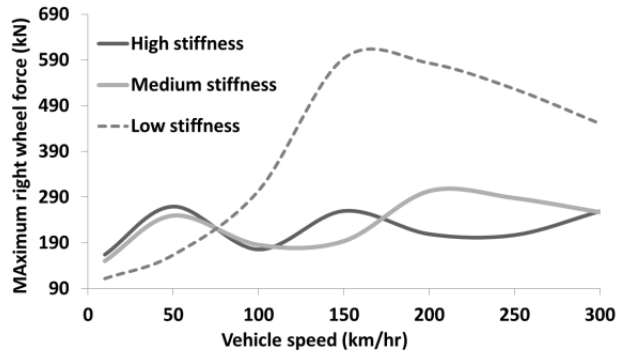

(a) Right wheel

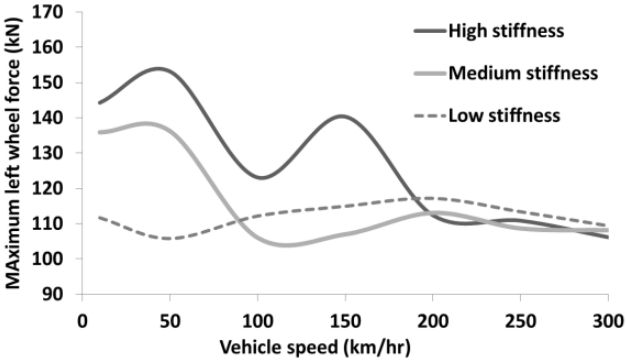

(b) Left wheel

Fig. 16 Maximum wheel/rail force of first wheel in asymmetric medium wheel-flat condition obtained from 3D model

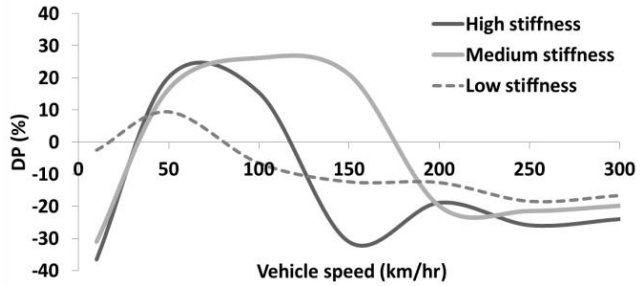

Fig. 17 DP in asymmetric large wheel-flat condition

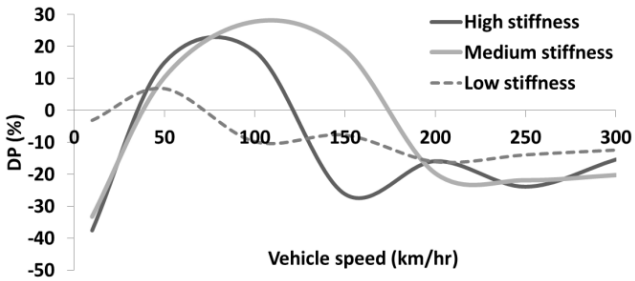

Fig. 18 DP in asymmetric very large wheel-flat condition

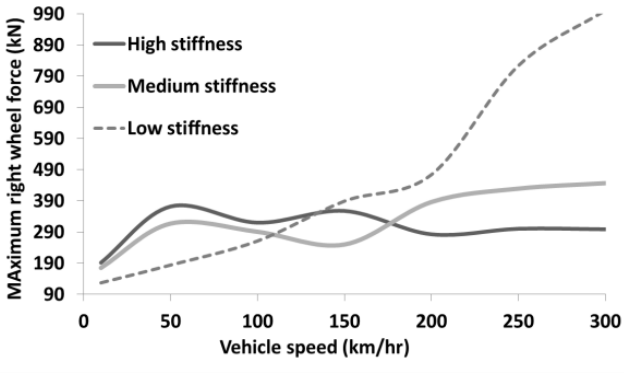

(a) Right wheel

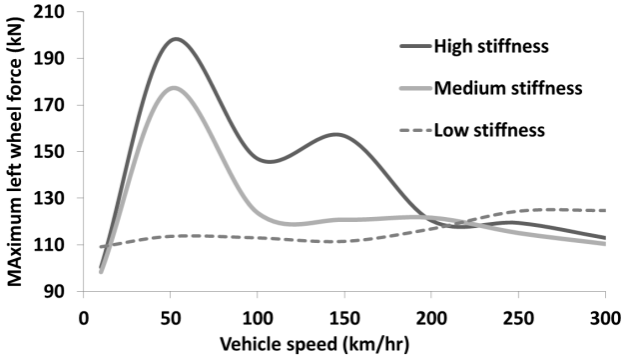

(b) Left wheel

Fig. 19 Maximum wheel/rail force of first wheel in asymmetric large wheel-flat condition obtained from 3D model

wheel. As a conclusion, in case of asymmetric medium wheel-flat condition, the accuracy of the results obtained from the 2D model is decreased, when the track stiffness is increased. Moreover, as the train speed is increased, the capability of the 2D model in prediction of the effects of medium asymmetric wheel-flat on the wheel/rail force is reduced.

The influences of large and very large wheel-flats on the DP are presented in Figs. 17 and 18, respectively. Moreover, the maximum wheel/rail force obtained from the 3D model in cases of large and very large wheel-flat conditions are presented in Figs. 19 and 20, respectively.

The general trend of the graphs presented in Figs. 17 and 18 are almost the same. The DP is reached to its maximum (40%) in the high stiffness when the vehicle speed is 10 m/hr, for both of large and very large wheel-flat conditions. When the train speed is more than 200 km/hr, the DP is slightly decreased compared to those of the train speed less than 200 km/r. As the track stiffness is decreased, the DP is decreased. As indicated in Figs. 19 and 20, the maximum wheel/rail force is reached to 900 kN and 1000 kN respectively in cases of large and very large asymmetric wheel-flat conditions. Figs. 19 and 20 indicate that the maximum wheel/rail force is intensified when the wheel-flat length and depth are increased.

From the results obtained in can be concluded that, the reliability of the 2D model in prediction of the effect of asymmetric wheel flat condition on the wheel/rail force is decreased when the wheel-flat length and depth are increased. As an interesting point, when the wheel-flat length and depth are increased, the variations of track stiffness and vehicle speed have a considerable effect on the DP variation. In other words, the accuracy of the results obtained from the 2D model is more reliable when the track

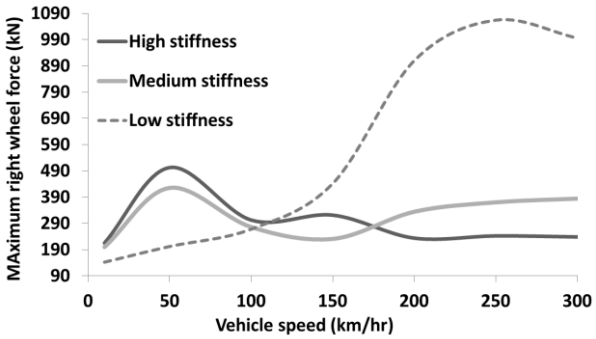

(a) Right wheel

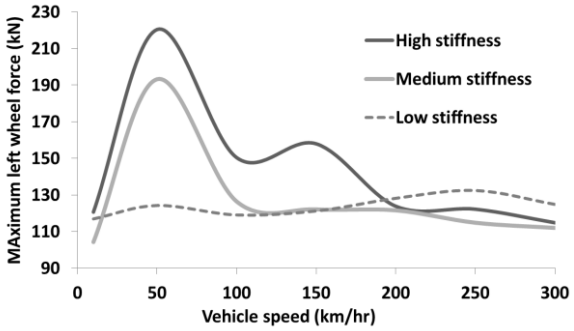

(b) Left wheel

Fig. 20 Maximum wheel/rail force of first wheel in asymmetric very large wheel-flat condition obtained from 3D model

Table 4 Wheel-flat ratios

Wheel flat condition	Wheel flat ratio
Small wheel flat	0.0025
Medium wheel flat	0.009
Large wheel flat	0.01
Very large wheel flat	0.01433

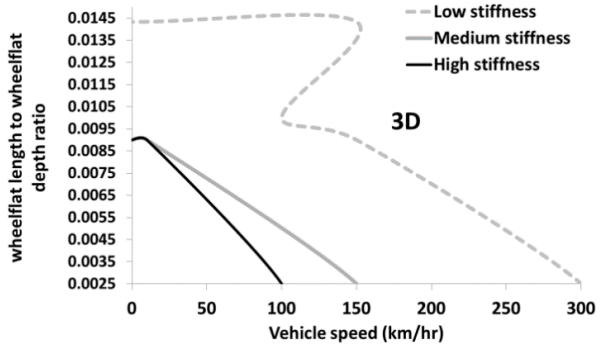

Fig. 21 Asymmetric wheel-flat optimum modeling technique threshold

stiffness is low and vehicle speed is less than 100 km/hr.

5. Optimum modeling technique

The computational cost of the 2D model was 84% lower than that of the 3D model in various conditions of the rail or the wheel (Zobrist and Ho 2000). As expected, the type of wheel-flat has no noticeable effects on the differences between the computational costs of both models. It is only dependent on the total time steps in the analysis and the total DOF of the models (Chen and Richard Liew 1995). Since the DOF of a 3D model is about 5 times more than that of a 2D model, the consuming time of the 2D model is about 150 times less than that of the 3D model (Chen and Richard Liew 1995). In the asymmetric wheel-flat condition, the results obtained from the 2D model are different than those of the 3D model. Based on the results presented in Figs. 13, 15, 17 and 18, the difference between the results obtained from the 2D model and the 3D model, is in the ranges of 0.03 to 40 percent. Therefore, in the asymmetric wheel-flat condition, a threshold can be derived in which the use of 2D modeling technique is justifiable. Based on the results discussed above, the wheel-flat characteristics, the train speed and the track stiffness are the dominant factors in the accuracy of the results obtained from the 2D model. The ratio of wheel-flat length to its depth (WFR) was taken as an index (Eq. (13)). As the WFR is increased, the maximum wheel/rail force is increased. The WFR for small, medium, large and very large wheel-flats are presented in Table 4.

$$WFR = \frac{Wheelflat\ Length}{Wheelflat\ Depth} \tag{13}$$

According to the literature (Chen and Richard Liew 1995), 10% errors in prediction of wheel/rail force is reasonably acceptable. Based on this suggestion, a threshold (bandwidth), in which the results of 2D model can be acceptable, was developed (Fig. 21). In this figure, the vehicle speed is drawn against the WFR for various track stiffness. The track stiffness level is considered as the contour. If the intersection point of the lines drawn from WFR (the Y axis) and the vehicle speed (the X axis) is placed under the contour line, the 2D model is optimum modeling technique; otherwise the 3D model should be used. This figure can be used as a guideline to adapt the best modeling technique in prediction of rail-wheel contact forces. The optimum modeling technique proposed in this study can be used in the simulation of the straight railway lines.

6. Conclusions

There is a controversy over the use of three or two dimensional models for prediction of the wheel/rail contact forces. While 2D models are cost-effective and less time consuming compared to 3D models, their accuracy is questionable particularly when the wheel has flatness. In fact, the wheel flat is an asymmetry phenomenon in the railways. Despite this fact, two dimensional (2D) models of railway vehicle/track interaction have been mostly used in the investigation of the effect of wheel-flats on the dynamic wheel-rail force in the literature. In this paper, cost effectiveness and the reliability of two dimensional models of railway vehicle/track interaction compared with three dimensional ones were investigated, leading to drive an

optimum modeling technique. Two 2D and 3D models of the vehicle/track interaction were developed. The validation of the results obtained from the 3D model was made by comparing the results with those obtained from a thorough filed investigation carried out in this research. Comparisons of the results obtained from the 2D and 3D models were made from two aspects: computational cost and accuracy of the results obtained.

Comparisons of the analyses times of the 2D and 3D model indicate that the computational cost of 2D models is considerably less (150 times) than that of the 3D model in all wheel flat cases. On the other hand, the accuracy of the results obtained from the 2D model in some track and wheel flat conditions have considerable errors. The difference between the results obtained from 2D and 3D models is between 0.03 to 40 percent. It was shown that the results of the 2D models are reliable for particular ranges of vehicle speed, railway track stiffness and wheel-fats lengths and depths. In case of asymmetric small wheel-flat condition and low track stiffness, the differences in the results obtained from 2D and 3D models are negligible in comparison with those of medium and high track stiffness. As the wheel/rail force is increased, the differences are increased. The difference between 2D and 3D model is increased when the wheel-flat size was changed from small to medium, large and very large. Also, as the track stiffness is increased, the difference is increased.

Using the results obtained, an optimum modeling technique for the investigation of the effect of single wheel flat on the wheel/rail force was derived by compromising between the accuracy and the computational cost. The optimum technique is presented in a diagram which takes into consideration the vehicle speed, the track stiffness and the ratio of wheel-flat length to wheel-flat depth. This diagram is a guideline for adapting an optimum modelling technique in the investigation of the effect of single wheel flat on the wheel/ rail force.

References

Askarinejad, H. and Dhanasekar, M. (2016), "A multi-body dynamic model for analysis of localized track responses in vicinity of rail discontinuities", *Int. J. Struct. Stab. Dyn.*, **16**(1), 1-33.

Borst, R., Crisfield, M.A., Remmers, J. and Verhoosel, C. (2012), *Nonlinear Finite Element Analysis of Solids and Structures*, John Wiley & Sons Ltd, London, U.K.

Chen, W. and Richard Liew, J. (1995), *The Civil Engineering Handbook*, CRC Press, New York, U.S.A.

CNR, C.R. (2002), *Car Manuals for Tehran Subway Line 1*, Changchun Railway Vehicles Co. Technical Report No 2.

Edem, I.B. (2006), "The exact two-node Timoshenko beam finite element using analytical bending and shear rotation interdependent shape functions", *Int. J. Comput. Meth. Eng. Sci. Mech.*, **7**(6), 425-431.

Egana, J.I., Vinolas, J. and Seco, M. (2006), "Investigation of the influence of rail pad stiffness on rail corrugation on a transit system", *Wear*, **261**(1), 216-224.

Gandhi, V.C., Kumaravelan, R., Ramesh, S. and Sriram, K. (2015), "Analysis of material dependency in an elastic-plastic contact models using contact mechanics approach", *Struct. Eng. Mech.*, **53**(5), 1051-1066.

Guo, T., Cao, Z., Zhang, Z. and Li, A. (2017), "Numerical simulation of floor vibrations of a metro depot under moving subway trains", *J. Vibr. Contr.*, **24**(18), 4353-4366.

Hamdoon, M., Zamaniand, N. and Das, S. (2011), "FEA of the blast loading effect on ships hull", *Ocean Syst. Eng.*, **1**(3), 223-229.

Handoko, Y. and Dhanasekar, M. (2006), "An inertial reference frame method for the simulation of the effect of longitudinal force to the dynamics of railway wheelsets", *Nonlin. Dyn.*, **45**(3), 399-425.

Jansseune, A. and De Corte, W. (2017), "The influence of convoy loading on the optimized topology of railway bridges", *Struct. Eng. Mech.*, **64**(1), 45-58.

Jia, S. and Dhanasekar, M. (2007), "Detection of rail wheel flats using wavelet approaches", *Struct. Health Monitor.*, **6**(2), 121-131.

Kahya, V. and Araz, O. (2017), "Series tuned mass dampers in train-induced vibration control of railway bridges", *Struct. Eng. Mech.*, **6**(2), 453-461.

Kouroussis, G., Connolly, D.P., Alexandrou, G. and Vogiatzis, K. (2015), "Railway ground vibrations induced by wheel and rail singular defects", *Vehic. Syst. Dyn.*, **53**(1), 1500-1519.

Kreiser, D., Jia, S.X., Han, J.J. and Dhanasekar, M. (2007), "A nonlinear damage accumulation model for shakedown failure", *Int. J. Fatig.*, **29**(8), 1523-1530.

Kumaran, G., Menon, D. and Nair, K. (2002), "Evaluation of dynamic load on rail track sleepers based on vehicle-track modeling and analysis", *Int. J. Struct. Stab. Dyn.*, **3**(1), 355-374.

Molatefi, H. and Izadbakhsh, S. (2013), "Continous rail absorber design using decay rate calculation in FEM", *Struct. Eng. Mech.*, **48**(4), 455-466.

Nasr, A., Mrad, C. and Nasri, R. (2018), "Friction tuned mass damper optimization for structure under harmonic force excitation", *Struct. Eng. Mech.*, **65**(6), 761-769.

Newton, S. and Clark, R. (1979), "An investigation into the dynamic effects on the track of wheel-flats on railway vehicles", *J. Mech. Eng. Sci.*, **4**(1), 287-297.

Nielsen, J. and Igeland, A. (1995), "Vertical dynamic interaction between train and track-influence of wheel and track imperfections", *J. Sound Vibr.*, **5**(1), 825-839.

Przemieniecki, J.S. (1985), *Theory of Matrix Structural Analysis*, Dover Publications, New York, U.S.A.

Sadeghi, J., Khajehdezfuly, A., Esmaeili, M. and Poorveis, D. (2016a), "Dynamic interaction of vehicle and discontinuous slab track considering nonlinear hertz contact model", *J. Transp. Eng.*, **142**(1), 1-11.

Sadeghi, J., Khajehdezfuly, A., Esmaeili, M. and Poorveis, D. (2016b), "Investigation of rail irregularity effects on wheel/rail dynamic force in slab track: Comparison of two and three dimensional models", *J. Sound Vibr.*, **374**(1), 228-244.

Sadeghi, J., Khajehdezfuly, A., Esmaeili, M. and Poorveis, D. (2016c), "An efficient algorithm for nonlinear analysis of vehicle/track interaction", *Int. J. Struct. Stab. Dyn.*, **16**(8), 1-20.

Sadeghi, J. and Fesharaki, M. (2013), "Importance of nonlinearity of track support system in modeling of railway track dynamics", *Int. J. Struct. Stab. Dyn.*, **13**(1), 1-16.

Shallan, O., Maaly, H.M. and Hamdy, O. (2018), "A developed design optimization model for semi-rigid steel frames using teaching-learning-based optimization and genetic algorithms", *Struct. Eng. Mech.*, **66**(2), 173-183.

Steenbergen, J.M.M. (2007), "The role of the contact geometry in wheel-rail impact due to wheel flats", *Vehicl. Syst. Dyn.*, **45**(12), 1097-1116.

Sun, Y. and Dhanasekar, M. (2002), "A dynamic model for the vertical interaction of the rail track and wagon system", *Int. J. Sol. Struct.*, **5**(1), 1337-1359.

Thompson, D., Wu, T. and Armstrong, T. (2003), "Wheel/rail

rolling noise- the effects of nonlinearities in the contact zone", *Proceedings of the 10th International Congress on Sound and Vibration*, Stockholm, Sweden, July.

Uzzal, R. (2012), "Analysis of a three-dimensional railway vehicle-track system and development of a smart wheelset", Ph.D. Dissertation, Concordia University of Canada, Montreal, Canada.

Uzzal, R., Ahmed, W. and Rakheja, S. (2008), "Dynamic analysis of railway vehicle-track interaction due to wheel flat with a pitch-plane vehicle model", *J. Mech. Eng.*, **2**(1), 86-94.

Uzzal, R., Stiharu, I. and Ahmed, W. (2009), "Design and analysis of MEMS based accelerometer for automatic detection of railway wheel flat", *World Acad. Sci. Eng. Technol.*, **1**(1), 792-800.

Uzzal, R., Ahmed, W. and Bhat, R. (2013), "Modeling, validation and analysis of a three-dimensional railway vehicle-track system model with linear and nonlinear track properties in the presence of wheel flats", *Vehic. Syst. Dyn.*, **11**(1), 1695-1721.

Uzzal, R., Ahmed, W. and Bhat, R. (2014), "Impact analysis due to multiple wheel flats in three-dimensional railway vehicle-track system model and development of a smart wheelset", *J. Rail Rap. Transit.*, **230**(2), 450-471.

Wu, T. and Thompson, D. (2004), "On the parametric excitation of the wheel/track system", *J. Sound Vibr.*, **3**(1), 725-747.

Xia, C., Ma, Q., Song, F., Wu, X. and Xia, H. (2018), "Dynamic analysis of high-speed railway train-bridge system after barge collision", *Struct. Eng. Mech.*, **67**(1), 9-20.

Yan, Q., Li, B., Deng, Z. and Li, B. (2018), "Dynamic responses of shield tunnel structures with and without secondary lining upon impact by a derailed train", *Struct. Eng. Mech.*, **65**(6), 741-750.

Yang, Y.B., Chang, J. and Yau, J. (1999), "A simple nonlinear triangular plate element and strategies of computation for nonlinear analysis", *Comput. Meth. Appl. Mech. Eng.*, **3**(1), 307-321.

Zhai, W., Wang, Q., Lu, Z. and Wu, X. (2001), "Dynamic effects of vehicles on tracks in the case of raising train speeds", *J. Rail Rap. Transit.*, **2**(1), 125-135.

Zhu, J.J., Ahmed, A.K.W., Rakheja, S. and Hu, Y.S.J. (2009), "Railway ground vibrations induced by wheel and rail singular defects", *Rail Rap. Transit.*, **223**(4), 391-403.

Zobrist, G. and Ho, C. (2000), *Intelligent Systems and Robotics*, Gordon and Breach Science Publisher, Australia.

Zou, Q., Deng, L., Guo, T. and Yin, X. (2016), "Comparative study of different numerical models for vehicle-bridge interaction analysis", *Int. J. Struct. Stab. Dyn.*, **16**(1), 1-28.

CC